Hypernuclear spectroscopy using the $(e, e'K^+)$ reaction

L. Yuan,[1] M. Sarsour,[2] T. Miyoshi,[3] X. Zhu,[1] A. Ahmidouch,[4] D. Androic,[5] T. Angelescu,[6] R. Asaturyan,[7] S. Avery,[1] O. K. Baker,[1,9] I. Bertovic,[5] H. Breuer,[8] R. Carlini,[9] J. Cha,[1] R. Chrien,[10] M. Christy,[1] L. Cole,[1] S. Danagoulian,[1] D. Dehnhard,[11] M. Elaasar,[12] A. Empl,[2] R. Ent,[9] H. Fenker,[9] Y. Fujii,[3] M. Furic,[5] L. Gan,[1] K. Garrow,[9] A. Gasparian,[1] P. Gueye,[1] M. Harvey,[1] O. Hashimoto,[3] W. Hinton,[1] B. Hu,[1] E. Hungerford,[2] C. Jackson,[1] K. Johnston,[14] H. Juengst,[11,18] C. Keppel,[1] K. Lan,[2] Y. Liang,[1] V. P. Likhachev,[14] J. H. Liu,[1] D. Mack,[9] A. Margaryan,[7] P. Markowitz,[15] H. Mkrtchyan,[7] S. N. Nakamura,[3] T. Petkovic,[5] J. Reinhold,[15] J. Roche,[16] Y. Sato,[3,1] R. Sawafta,[4] N. Simicevic,[13] G. Smith,[9] S. Stepanyan,[7] R. Sutter,[10] V. Tadevosyan,[7] T. Takahashi,[3] K. Tanida,[17] L. Tang,[1,9] M. Ukai,[3] A. Uzzle,[1] W. Vulcan,[9] S. Wells,[13] S. Wood,[9] G. Xu,[2] H. Yamaguchi,[3] and C. Yan[9]

(HNSS Collaboration)

[1]*Hampton University, Hampton, Virginia 23668, USA*
[2]*University of Houston, Houston, Texas 77204, USA*
[3]*Tohoku University, Sendai, 980-8578, Japan*
[4]*North Carolina A&T State University, Greensboro, North Carolina 27411, USA*
[5]*University of Zagreb, Zagreb, Croatia*
[6]*University of Bucharest, Bucharest, Romania*
[7]*Yerevan Physics Institute, Yerevan, Armenia*
[8]*University of Maryland, College Park, Maryland 20742, USA*
[9]*Thomas Jefferson National Accelerator Facility, Newport News, Virginia 23606, USA*
[10]*Brookhaven National Laboratory, Upton, New York 11973, USA*
[11]*University of Minnesota, Minneapolis, Minnesota 55455, USA*
[12]*Southern University at New Orleans, New Orleans, Lousiana 70126, USA*
[13]*Louisiana Tech University, Ruston, Lousiana 71272, USA*
[14]*University of Sao Paulo, Sao Paulo, Brazil*
[15]*Florida International University, Miami, Florida 33199, USA*
[16]*College of William and Mary, Williamsburg, Virginia 23187, USA*
[17]*University of Tokyo, Tokyo 113-0033, Japan*
[18]*Old Dominion University, Norfolk, Virginia 23529, USA*

(Received 10 August 2004; revised manuscript received 12 July 2005; published 11 April 2006)

A pioneering experiment in Λ hypernuclear spectroscopy, undertaken at the Thomas Jefferson National Accelerator Facility (JLab), was recently reported. The experiment used the high precision, continuous electron beam at JLab, and a special arrangement of spectrometer magnets to measure the hypernuclear spectrum from C and ^{7}Li targets using the $(e, e'K^+)$ reaction. The $^{12}_{\Lambda}$B spectrum found in this investigation was previously published, but is reported here in more detail, with improved resolution. In addition, the results of a $^{7}_{\Lambda}$He spectrum also obtained in the experiment, are shown. This latter spectrum indicates the need for a more detailed few-body calculation of the hypernucleus and the reaction process. The success of the experiment demonstrates the potential of the $(e, e'K^+)$ reaction for high resolution spectroscopy of hypernuclear spectra.

DOI: 10.1103/PhysRevC.73.044607 PACS number(s): 21.80.+a, 21.10.Dr, 21.60.Cs

I. INTRODUCTION

The introduction of strangeness into the nuclear medium challenges conventional models of this low-energy, hadronic, many-body system. Of particular interest is the fact that in the single-particle model of the nucleus the Λ can be used to probe the nuclear interior, as it is not excluded by the Pauli principle from occupying interior shells.

The effective Λ-nucleus potential is weaker and shorter ranged than that for a nucleon, since one pion exchange (OPE) between a Λ and a nucleon does not occur due to the conservation of isospin. Thus the ΛN potential is obtained from higher mass meson exchanges, including the two-pion exchange coupling through an intermediate sigma ($\Lambda N \Leftrightarrow \Sigma N$), and this leads to sizable charge asymmetry and three-body forces [1]. In addition, the strangeness degree of freedom allows the nucleus to rearrange by taking advantage of SU(3) flavor symmetry, in order to maximize the nuclear binding energy [2]. For these reasons the hypernuclear system can better illuminate various nuclear features which are more obscured in conventional nuclear hadrodynamics.

The hypernuclear system also provides a method to extract the parameters of a generalized model of the elementary Λ-nucleon potential, which is presently impossible to accurately determine directly by hyperon-nucleon scattering. Since, the ΛN interaction is weak, one can with some confidence, relate the parameters of a ΛN potential to those of an effective Λ-nucleus single-particle interaction fitted to the experimental hypernuclear spectra [3]. Such information would then illuminate the $SU(3)_{\text{flavor}}$ baryon-baryon interaction at

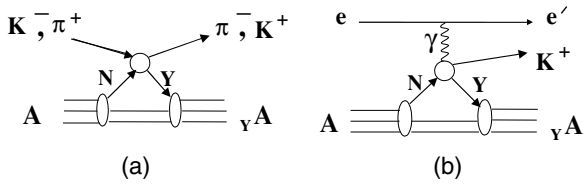

FIG. 1. A schematic representation of the (a) mesonic and (b) electromagnetic production processes.

normal nuclear densities, and this information can serve as a normalization point, to extrapolate the interaction to matter-densities found in neutron stars, where mixtures of nucleons and hyperons could form a stable system [4].

Traditionally, hypernuclei have been produced with secondary beams of kaons or pions, as shown in Fig. 1(a). Because the (K^-, π^-) reaction is exothermic, the three-momentum transfer to the Λ can be chosen to be small. In this situation the cross section to substitution states (i.e., states where the Λ acquires the same shell quantum numbers as those of the neutron which it replaces) is relatively large. On the other hand, the (π^+, K^+) reaction has three-momentum transfers comparable to the nuclear Fermi-momentum, and the cross section preferentially populates states with high angular momentum transfers [5,6]. Neither of these two reactions has significant spin-flip amplitude at forward angles where the cross sections are experimentally accessible. Thus all these spectra are dominated by transitions to non-spin-flip states.

Aside from early emulsion experiments, mesonic reaction spectroscopy of hypernuclei has generally provided hypernuclear spectra with energy resolutions $\geqslant$2 MeV. This is due to the intrinsic resolutions of secondary mesonic beamlines, and the target thicknesses required to obtain sufficient counting rates. One previous study did achieve a spectrum resolution of approximately 1.5 MeV for the ${}_{\Lambda}$C hypernucleus, using a thin target and devoting substantial time to data collection [7].

Although, specific hypernuclear states below nucleon emission threshold can be located within $\leqslant$1 keV by detecting deexcitation gammas [8,9] in coincidence with a hypernuclear production reaction, such experiments become more difficult in heavier systems due to the number of transitions which must be unambiguously assigned in an unknown spectrum. It should be noted however, that resolutions of a few hundred keV are also sufficient for many studies, since reaction selectivity and angular dependence potentially allows extraction of the spectroscopic factors to specific states [10]. A reaction also provides a full spectrum of states which can be clearly identified with a specific hypernucleus. Indeed the excitation strength of the spectrum is of interest, as the impulse approximation assumes that the reaction proceeds through the interaction of the incident projectile with a nucleon in a single-particle state within the nuclear medium. Thus as an example apropos to the experiment reported here, if the theoretical spectrum does not reproduce the experimental one, it is possible that propagator renormalization within the medium could be significant [11], requiring a modification of the single-particle picture of the reaction.

Electroproduction of hypernuclei is illustrated by Fig. 1(b). Electroproduction traditionally has been used for precision studies of nuclear structure, as the exchange of a photon can be accurately described by a first order perturbation calculation. In addition, electron beams have excellent spatial and energy resolutions. Previously, electron accelerators had poor duty factors, significantly impairing high singles rate, coincidence experiments. However, modern, continuous beam accelerators have now overcome this limitation, and although the cross section for nuclear kaon electroproduction is smaller than that for hypernuclear production by the (π, K) reaction for example, this can be compensated by increased beam intensity. Targets can be physically small and thin (10–100 mg cm^{-2}), allowing studies of almost any isotope. The potential result for $(e, e'K^+)$ experiments, is an energy resolution of a few hundred keV with reasonable counting rates up to at least medium weight hypernuclei [12].

The $(e, e'K^+)$ reaction, because of the absorption of the spin 1 virtual photon, has high spin-flip probability even at forward angles. In addition, the three-momentum transfer to a quasifree Λ is high, approximately 300 MeV/c at 0° for 1500 MeV incident photons, so the resulting reaction is expected to predominantly excite spin-flip transitions to spin-stretched states [13]. Spin-flip states are not strongly excited in hadronic production, and the $(e, e'K^+)$ reaction acts on a proton rather than a neutron, creating proton-hole, Λ-particle states, charge symmetric to those previously studied with meson beams. Precision experiments, comparing mirror hypernuclei, are needed in fact, to extract the charge asymmetry in the ΛN potential.

An initial experiment [14], in Hall C at Thomas Jefferson National Acceleration Facility (JLab) has been previously reported, and this paper discusses the experiment in more detail, presenting an improved ${}_{\Lambda}$B spectrum as well as a previously unpublished spectrum of the ^{7}Li$(e, e'K^+)^7_{\Lambda}$He reaction.

II. EXPERIMENTAL DETAILS

In electroproduction, the Λ and K^+ particles are created associatively via an interaction between a virtual photon and a proton in the nucleus, $p(\gamma, K^+)\Lambda$. The hypernucleus, ${}_{\Lambda}A$, is formed by coupling the Λ to the residual nuclear core, (Z-1), as shown in Fig. 1(b). In electroproduction, the energy and three-momentum of the virtual photon are defined by $\omega = E_e - E_e^{'}$ and $\vec{q} = \vec{p}_e - \vec{p}_e^{'}$, respectively. The square of the four-momentum transfer of the electron is then given by $-Q^2 = t = \omega^2 - q^2$.

As will be shown below, the number of (virtual) photons falls rapidly as the scattered electron angle increases (increasing t), and thus the distribution of (virtual) photons also peaks in the forward direction. In addition, the nuclear transition matrix element causes the cross section for hypernuclear production to fall rapidly with the angle between the reaction kaon and the (virtual) photon. Thus experiments must be done within a small angular range around the direction of the incident electron. To accomplish this, the experimental geometry requires two spectrometer arms, one to detect the

scattered electron and one to detect the kaon, both placed at extremely forward angles.

The electroproduction cross section can be expressed [15] by

$$\frac{\partial^3\sigma}{\partial E_e' \partial\Omega_e' \partial\Omega_K} = \Gamma\left[\frac{\partial\sigma_T}{\partial\Omega_K} + \epsilon\frac{\partial\sigma_L}{\partial\Omega_K} + \epsilon\cos(2\phi) \times \frac{\partial\sigma_{TT}}{\partial\Omega_K} + \cos(\phi)\sqrt{2\epsilon(1+\epsilon)}\frac{\partial\sigma_{LT}}{\partial\Omega_K}\right].$$

Thefactor, Γ, is the virtual flux factor evaluated with electron kinematics in the lab frame, and ϕ is the angle measuring the out-of-plane production of the kaon with respect to the plane containing the beam and scattered electron. The factor, Γ, has the form

$$\Gamma = \frac{\alpha}{2\pi^2 Q^2}\left[\frac{E_\gamma}{1-\epsilon}\right]\frac{E_e'}{E_e}.$$

In the above equation, ϵ is the polarization factor, $E_\gamma = \omega$, and α is the fine structure constant;

$$\epsilon = \left[1 + \frac{2|\mathbf{q}|^2}{Q^2}\tan^2(\theta_e/2)\right]^{-1}.$$

The label on each of the cross section expressions (T, L, TT, and LT) represent transverse, longitudinal, polarization, and interference terms. For real photons of course, $Q^2 = 0$, so only the transverse cross section is nonvanishing, and for the experimental geometry used here, the virtual photons are almost on the mass shell, $Q^2 = p_\gamma^2 - E_\gamma^2 = 0$ so the cross section is completely dominated by the transverse component. Thus the electroproduction cross section may be replaced, to good approximation, by the photoproduction value multiplied by the flux factor.

Experimentally, Γ is integrated over the angular and momentum acceptances of the electron spectrometer. In order to maximize the cross section of the elementary, $p(\gamma, K^+)\Lambda$ reaction, the photon energy is chosen to be about 1.5 GeV. In addition, to keep strangeness production limited essentially to kaons and Λs, the energy, E_e, of the incident electron is chosen to be approximately $\leqslant$1.8 GeV. In this way, backgrounds from unwanted reactions are reduced. This also allows a physically small, low-momentum electron spectrometer to be employed, as the scattered electron energy, E_e', is about 0.3 GeV.

Figure 2 shows the calculated virtual photon flux factor in units of photons per electron per MeV sr for the chosen kinematics. This flux factor peaks at zero degrees and falls rapidly as the scattering angle increases [16,17]. With electrons detected at 0°, a large percentage of the scattered electrons are captured by even a small solid angle, increasing the coincidence probability between these electrons and the reaction kaons of interest. In addition, because of the small beam spot ($\approx$100 μm), the $\approx$0° to 4° electron scattering angle, and the small momentum value of the scattered electron, it is sufficient to measure only the electron position on the spectrometer focal plane to ensure excellent energy resolution. However, the disadvantage of this geometry is a high electron background rate from target bremsstrahlung, which ultimately limits the usable beam luminosity.

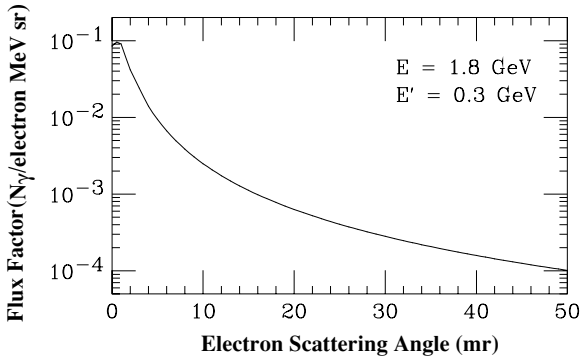

FIG. 2. The virtual photon flux factor as a function of the electron scattering angle.

Once the choice of the incident and scattered electron momenta is fixed, the production kaon momenta are determined by the kaon production angle. In this experiment, the chosen kinematics produced a kaon momentum of $\approx$1.2 GeV/c, providing a three-momentum transfer of $\approx$300 MeV/c to the recoiling Λ. The kaon momentum provides a reasonable kaon survival fraction, and allows π/K discrimination using threshold aerogel Cerenkov detectors coupled with time of flight. Fig. 3 shows a schematic view of the experimental layout.

A. The beam

The beam has a bunch width of 1.67 ps with a bunch separation of 2 ns. While the absolute value of the energy of the incident electrons was unimportant (although for kinematic reasons to be discussed below, it did need to be determined), it was extremely important to precisely maintain whatever this energy was over the several weeks of the experiment. Thus the beam momentum is locked by a *fast feedback energy lock* system installed in an arc of the accelerator. This system measured, at a repetition rate of 1 kHz, the beam parameters at

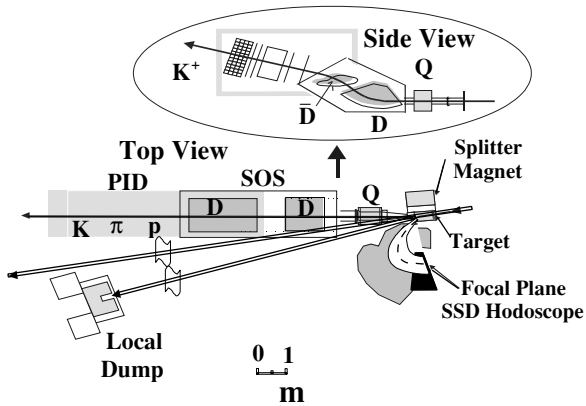

FIG. 3. The experimental plan view showing both the kaon spectrometer (SOS) and the electron spectrometer (ENGE). The SOS is a QDD spectrometer with Q an entrance quadrupole, and DD two dipoles bending in opposite directions, providing large momentum acceptance but reducing dispersion.

the entrance, the position of maximum momentum dispersion, and the exit of the arc, to extract an energy correction factor. This correction was then applied to the last cavity of the accelerator, maintaining a constant beam energy. The feedback lock controlled the average energy of the primary electron beam to a $\delta p/p \leqslant 10^{-4}$. The intrinsic energy spread about a given average energy was controlled by tuning the spread in the injected energy.

A similar lock system maintained the beam position on target within 100 μm. Although the intrinsic spot size was tuned to be $\leqslant 100$ μm, the beam was rastered over a 4×4 mm^2 area when incident on the CH_2 target, to reduce beam heating. The beam position on target was measured and used in the analysis of the calibrations and data in order to correct the resolution for variations in the position of the target spot.

Beam intensities were set to produce an acceptable signal to accidental ratio of $\geqslant 0.6$. The intensity for the C target was approximately 0.6 μA, or an experimental luminosity of approximately 4×10^{33} cm^{-2} s^{-1}. Due to the lower radiation length of the ^{7}Li target, a higher beam current of about 0.8 μA was used. To protect the CH_2 target, the beam current for this target was kept below 1.5 μA.

Finally, to satisfy scheduling constraints the experimental data was acquired at two different beam times with two different beam energies, 1721 and 1864 MeV. These different energy data were analyzed separately, but the kinematical conditions for the two beam energies were close, and the spectra showed no energy dependence within statistics. Therefore these data were summed after separate analysis to increase the statistical significance of the final spectrum. In addition to calibrations, about 400 h of data were collected with the C target and about 120 h with the ^{7}Li target.

B. The splitting magnet and targets

In order to detect both scattered electrons and positively charged kaons near zero degrees, a C magnetic dipole (splitter) was used. The target was positioned at the upstream side of the effective field boundary of this magnet. The splitter deflected electrons scattered at approximately 0° and kaons at approximately 2° by 33° and 16°, respectively.

Three different, target foils were employed, CH_2, 8.8 mg cm^{-2}, C, 22 mg cm^{-2}, and ^{7}Li, 19 mg cm^{-2}. By observing the $p(e, e'K^+)\Lambda$ and $p(e, e'K^+)\Sigma$, the hydrogen in the CH_2 foil was used for energy calibration and optimization of the spectrometer optics. These procedures are described in the subsections below.

C. The kaon spectrometer

A short orbit spectrometer (SOS) is one of two existing magnetic spectrometers in Hall C at JLab, and as it has a flight path of $\approx$10 m, this spectrometer is particularly useful for the detection of particles with short half-lives. However, it has low dispersion and large momentum acceptance, and these characteristics are not well matched to the present experimental geometry. Nevertheless, because the SOS was mounted at the Hall C pivot and had the sophisticated particle identification (PID) package [18] required to identify kaons within the large background of pions and positrons, it was chosen as the kaon spectrometer for this first $(e, e'K^+)$ experiment. It was expected that the overall resolution would be dominated by this spectrometer [22].

The solid angle acceptance of the splitter/SOS spectrometer system was approximately 5 msr, covering a range of scattering angles from 0° to 4°. The error in the reconstructed kaon reaction angle was about 13 mr (FWHM), and was dominated by the horizontal angular measurement error. This contributed about 200 keV to the missing mass resolution when the atomic number of the recoiling hypernucleus was $\geqslant 6$. The central momentum of the SOS was set to 1.2 GeV/c. The momentum acceptance was $\approx$46%, but only the central $\pm$15% was useful. This acceptance was nearly flat within the missing mass range of interest.

The standard SOS detector package was used. It consisted of (1) two sets of tracking chambers separated by 0.5 meters; (2) four scintillation hodoscope planes; (3) one aerogel Cerenkov (AC) counter with an optical index of 1.03; (4) one lucite, total internally reflecting Cerenkov (LC) counter with index 1.49; (5) one gas Cerenkov (GC) detector; and (6) three layers of lead-glass shower counters. The tracking detectors were used to determine the position and angle of the particle on the focal plane, and by projection, its production angle from the target. The scintillator hodoscopes were used to localize tracks in the wire chambers, and to obtain timing and time of flight (TOF) information for PID. The aerogel Cerenkov detector was used to veto pions and positrons, and the lucite counter was used to remove protons by tagging high-beta particles. The gas Cerenkov detector and the lead-glass shower counters were used to remove positrons.

D. The electron spectrometer

The scattered electrons were detected in a split-pole, magnetic spectrometer (ENGE) [19], which was well matched to the geometrical kinematics and acceptances. The spectrometer coupled with the phase space of the incident beam, had the capability of obtaining 5×10^{-4} resolution (FWHM $\delta p/p$). The central momentum was chosen to be 300 MeV/c with a momentum acceptance of $\approx$120 MeV/c. The solid angle acceptance of the combined splitter/split-pole system was about 9 msr, which effectively tagged about 35% of the virtual photon flux for 1.5 GeV photons. The spread in the (virtual) photon momentum was $\approx$120 MeV/c, centered around $\approx$1500 MeV/c. In summary, the geometry of the electron arm was possible because of the excellent phase space of the incident electron beam, the thin targets which limited multiple scattering, and the extremely forward peaking of the virtual photon flux factor.

However, target bremsstrahlung also peaks at 0° and large numbers of scattered electrons are expected to enter the split-pole spectrometer [16]. In fact the experimental luminosity was set by accepting a total rate of $\approx 2 \times 10^8$ s^{-1} on the instrumented portion of the focal plane. Tracking at the expected singles rates would have resulted in many ambiguous trajectories. However the choice of the spectrometer, electron momenta,

and scattering geometry required only a measurement of the focal plane position of a scattered electron in order to obtain the required resolution. The focal plane detector [20] was composed of ten, one-dimensional silicon strips segments (SSD), each having 144 strips with a pitch of 0.5 mm and length of 5 cm. These segments were placed approximately perpendicular to the electrons, which were incident on the focal plane at $\approx 47^\circ$ over a length of 72 cm. The singles rate per strip was on average $\approx 10^5$ s^{-1}.

A set of eight scintillation strip counters in a hodoscope arrangement were positioned directly behind each of the SSD segments. These strips were 1 cm wide, 6 cm long, and 0.4 cm thick, viewed at one end through a light guide by a 3469 Hamamatsu photomultiplier. Rates per scintillator were found to be $\leqslant 1.5 \times 10^6$ s^{-1}, and no change in time resolution was observed up to rates $\leqslant 2.5 \times 10^6$ s^{-1}. The SSD provided the position of an electron event to within 500 μm and the scintillation hodoscope provided event timing to 250 ps (σ).

E. Pion/kaon discrimination

It was expected that the numbers of positrons, pions and protons in the SOS would be very much larger than the number of kaons. Indeed the measured rate of positrons, pions, protons, and kaons from the C target, was 10^5 s^{-1}, 1.4×10^3 s^{-1}, 140 s^{-1}, and 0.4 s^{-1}, respectively. Therefore excellent particle identification was required, not only in the analysis, but also in the hardware trigger.

The standard SOS detector package was used to identify kaons, and its description and operation have been previously discussed [18]. The large flux of positrons was due to the acceptance of scattering angles down to 0°, where positrons from Dalitz pairs, created in the target, were observed. Positrons were easily identified and could have been removed in the trigger by the lead-glass shower counter, but detection of the Dalitz pairs provided a useful confirmation of the experimental resolution.

The coincident time resolution between an electron and a kaon was 230 ps (FWHM), after pulse height and path length corrections were applied. After other kaon PID cuts were applied (i.e., Cerenkov threshold pion and proton vetoes and shower counter veto), the difference between the particle velocity as measured by the TOF between the scintillator hodoscopes in the SOS detector package and the velocity obtained from the measured momentum, is plotted as a function of the SOS path length corrected TOF in Fig. 4. In this plot, the velocity, $\beta_{\mathrm{mom}} = \frac{pc}{\sqrt{(pc)^2+(m_k c^2)^2}}$ uses the momentum measured by the spectrometer and assumes the mass is always equal to that of a kaon. The TOF between the fixed scintillation hodoscope planes in the SOS PID package uses the path length of the particle trajectory between the hodoscopes, ΔL, and the time, ΔT, to obtain, β_{TOF}. The difference, $\Delta\beta$, is used to place events on the vertical axis

$$\Delta\beta = \frac{\Delta L}{\Delta T} - \frac{pc}{\sqrt{(pc)^2 + (m_k c^2)^2}}.$$

This vertically separates particles of different mass into bands whose width is determined by the momentum bite in the spectrometer. For particles of 1200 MeV/c, pions are displaced by a $\Delta\beta$ of 0.07 above kaons, protons are displaced by 0.2 lower than the kaons. The horizontal axis is the path length corrected coincidence timing which imprints the time structure of the beam.

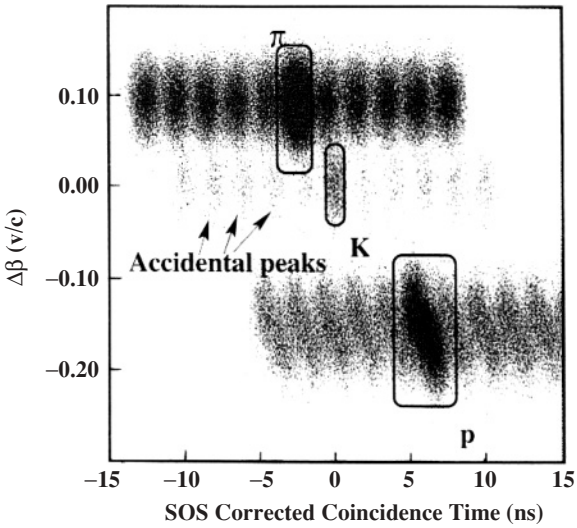

FIG. 4. A plot of SOS particle velocity vs the electron-kaon time-of-flight showing the separation of pions, kaons, and protons.

This structure is reproduced in Fig. 4. Thus the figure shows that the real kaon coincidences can be selected by applying a coincidence window 2 ns wide. Events selected from an average of eight nearby accidental coincidence windows were used to obtain the shape and magnitude of the accidental background spectrum.

F. The expected system resolution

Since the entire beamline/spectrometer system was under vacuum, multiple scattering in the air and vacuum windows occurred only at the exit of the spectrometers. Vacuum windows were located immediately before the first tracking detectors so that this effect on the measured track-position was minimized. Table I lists the expected contributions to the energy resolution. As discussed above, the contribution from the SOS spectrometer was expected to dominate. The system resolution was obtained by addition of the various contributions in quadrature.

TABLE I. Contributions to the system energy resolution.

Source	Contribution	Resolution (keV)
Beam energy	10^{-4}	$\leqslant 180$
SOS momentum	5.5×10^{-4}	≈ 660
Split-pole	5×10^{-4}	150
Kaon production angle (^{12}C)	13 mr	≈ 200
Target energy loss (^{12}C)	1.7 keV mg^{-1} cm^{-2}	38
Total		≈ 757

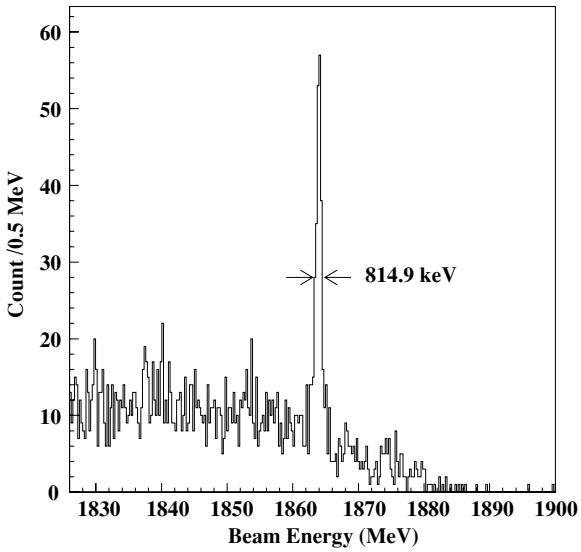

FIG. 5. Reconstructed beam energy from the measurement of Dalitz pairs detected by the spectrometer system. As described in the text, this was used to confirm the energy resolution of the experiment. The bin width is 0.5 Mev.

The system resolution could be experimentally checked using Dalitz pairs from the $A(e, e'; (e^+e^-))A$ reaction, where both electrons were detected in the electron spectrometer and the positron in the kaon spectrometer. As the electrons and positrons are emitted essentially at 0° and the electron mass is negligible, the sum of the separate energies of these particles is equal to the beam energy. The width of the reconstructed beam-energy peak, as obtained by a Gaussian fit to the Dalitz pair peak in Fig. 5 is about 815 keV (FWHM). Unfortunately the kinematics limited the electron pair to the upper region of the momentum acceptance of the ENGE spectrometer, where the resolution is maximized. However, from an optical study of the resolution over the entire focal plane, we estimate that the reconstructed energy should be approximately 900 keV (FWHM) and we believe this is sufficiently close to the measured value that an estimate of the experimental resolution can be obtained by removal of the contribution of one of the electrons from the measured experimental value of 815 keV. This generates our quoted experimental resolution of 750 keV FWHM, which is consistent with the width of the peak of the $^{12}_{\Lambda}$B experimental ground state doublet to be discussed below. The experimental Dalitz pair spectrum is shown in Fig. 5.

G. Rates and background

The singles rate in the electron arm was set to about 2×10^8 s^{-1}. As discussed previously, this rate was primarily a result of bremsstrahlung electrons. Therefore, the experimental trigger was chosen to be the observation of a kaon in the SOS spectrometer which occurs at a much lower rate. The coincidence spectra were then obtained later in off-line analysis. The positrons from e^+/e^- pair production dominated the rate in the kaon spectrometer. These Dalitz pairs were produced essentially at 0°, and since the SOS acceptance covered 0° to 4°, they were accepted into the spectrometer. However, the combined use of vetoes from AC, GC, and shower counters substantially reduced events triggered by positrons, and they were completely eliminated in the off-line analysis. Rates from protons and pions were also reduced to approximately 1 kHz after on-line cuts by the AC and LC detectors. The remaining protons and pions were also eliminated in the off-line analysis.

About 95% of the background observed in the raw spectra was due to accidental coincidences. An evaluation of this background began by obtaining a spectrum of the time difference between the emission of the kaon and electron(s) in an event. This time spectrum contained both the real, and a number of accidental peaks, separated by the 2 ns time structure in the beam. The summation of the analyzed spectra from eight of the accidental time-peaks provided a higher statistics measurement of the accidental background. The remaining background (5%) was due to real coincidences of pions (misidentified as kaons) with electrons. The TOF separation between pions and kaons was about 2 ns, and therefore coincidences could occur between electrons and the pions which were emitted 2 ns later but arrived in the time window of the real kaon peak. The shape of the pion background in the missing-mass spectra was obtained by cutting on pions in the PID and analyzing coincident pions assuming $(e, e'K^+)$ kinematics. The absolute magnitude of this background was then obtained by normalizing the pion spectrum to the number of background events.

In addition, the time resolution of $\sigma \approx 230$ ps allowed the tails of the real kaon coincidence peak to overlap with an accidental neighbor. Thus to calculate the cross section, the number of true coincident kaons lost from the real time peak was compensated by a cut-efficiency factor.

H. Calibrations, spectrometer optics, and kinematics

Calibration of the spectrometers requires knowledge of the magnetic transport coefficients. Although the coefficients for the SOS transport have been previously established in several experiments, the addition of the splitting magnet to the system requires that they be redetermined. To illustrate this point, the angular acceptance of the SOS, normally 7 msr for a point target, was reduced to 5 msr by the splitter.

In general, the reconstructed missing mass of a hypernuclear state, M_Y, is a function of the beam energy, E_e, the three-momenta of the scattered electron, $p_{e'}$, and kaon, p_K, and the angles $\theta_e, \theta_K, \delta\phi_{eK}$. These seven parameters are related by energy-momentum conservation, leaving an equation of three variables if the incident energy, and angles are known. The solutions to this equation form a set of loci in the two-dimensional space defined by the electron and kaon momenta. That is, a line for each hypernuclear mass defined by p_k as a function of $p_{e'}$. The momentum dependence of the cross sections and final state interactions influences the distribution of events along a given locus for a specific hypernuclear mass, M_Y. For the geometry used in this experiment where the cross section is expressed in terms of an energy averaged on-shell photoproduction cross section, experimental events

are projected onto, and summed along this locus, for a specific hypernuclear mass.

However the incident momenta and angles are not precisely known, although they are assumed to be constant during a set of experimental runs. Therefore using an incorrect value of the beam momentum or angles for either spectrometer arm, results in an incorrect knowledge of the position and slope of the locus line for a specific hypernuclear mass, and this results in an energy shift and spread in width of a hypernuclear state. Thus one needs not only to obtain a focal-plane-to-momentum calibration for the spectrometers, but in principle to obtain a value of the beam energy and the reaction angles of the spectrometers. However, for the very forward angles and very low momentum transfers used in this experiment, the error introduced by the uncertainty in the spectrometer angles is negligible, so that the number of independent parameters for which calibrations must be found is reduced to 3, E_e and the central values of $p_{e'}$ and p_K. In addition, the beam energy remains near a nominal value for some accelerator setting, so that variations in this energy can be treated perturbatively. We have now obtained better calibration parameters than those used in the analysis of our previously reported $^{12}_{\Lambda}$B spectrum. This newer analysis incorporates the calibration of the above three parameters in a global fit to known hypernuclear masses as described below.

The simulation of charged particle trajectories through the system of magnets and detectors used the program, RAYTRACE [21]. The coefficients of the RAYTRACE code for the SOS spectrometer were determined by adjusting the splitter contribution so that the calculated multidimensional, phase-space distributions from a point beam matched those measured when the entrance angles and positions of reaction protons and pions from the target were restricted by a set of appropriately positioned holes in a tungsten plate (sieve slit) located between the splitting magnet and the SOS [22]. Optimization of the SOS coefficients used a χ^2 minimization process defined by the difference between the simulated and observed experimental patterns. This provides an initial central momentum and reaction angle calibration for this spectrometer.

The calibration procedure then used an initial set of transport parameters for the SOS-splitter spectrometer obtained from knowledge of the magnetic fields, to find an initial focal plane calibration for the ENGE spectrometer. Adjustments to the central momentum of the spectrometers were then made to simultaneously match the correct kinematic positions and widths of the Λ and Σ peaks as produced in the $p(\gamma, K^+)Y$ reaction, Fig. 6. This still left unspecified an adjustment to the absolute beam energy, and this parameter was obtained by a series of iterations. The latter was done by minimizing the deviations in the fit to the Λ and Σ peaks by varying the beam energy while keeping the central momentum values of the spectrometers constant. The optimum beam energy, as determined independently for the energies of the two experimental runs, was shifted downward by approximately 0.078% (-1.358 MeV for the 1.721 Gev beam and -1.455 MeV for the 1.864 GeV beam).

After obtaining a set of beam energy and central momentum values, the transport coefficients were refitted to the sieve slit data, and the ENGE focal plane calibration was redetermined. The fitting procedure also checked that the width of the ground state doublet excitation, obtained in the ^{12}C$(\gamma, K^+)^{12}_{\Lambda}$B reaction, was reasonable, i.e., within the experimental resolution.

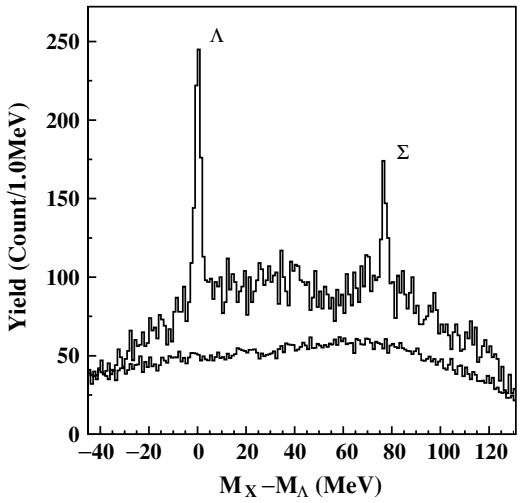

FIG. 6. The missing mass spectrum obtained from a CH_x target showing both Λ and Σ production from hydrogen in the target. The solid histogram is the accidental background. The bin width was 1.0 Mev.

Residual mass shifts of $\leqslant 200$ keV were obtained, and these were dominated by statistical errors on the estimates of the peak positions. The peak widths were in good agreement with a Monte Carlo simulation having the same statistics and background levels as the data.

From this more extensive calibration, the analysis produces peak widths of 2.8 MeV, 2.1 MeV and 0.75 MeV for the Λ, Σ, and ground state doublet of $^{12}_{\Lambda}$B, respectively. The previously reported values [14] were, 3.5 MeV, 2.7 MeV, and 0.90 MeV. It is estimated that the new calibration procedure produces a 300 keV error in the determination of the missing mass scale over the 130 MeV spectrometer acceptance.

The broad distribution above background and below the Λ missing mass as seen in Fig. 6 was due to hyperon production from the C in the target. Unfortunately during the extended calibration runs, H was removed from the target by beam heating so that the C to H ratio changed. Thus a direct normalization using the known $p(\gamma, K^+)\Lambda$ cross section could not be applied.

III. EXPERIMENTAL RESULTS AND DISCUSSION

The experiment obtained data for both $^{12}_{\Lambda}$B and $^{7}_{\Lambda}$He hypernuclei. The $^{12}_{\Lambda}$B spectrum was reported earlier. Subsequently the spectrometer transport and calibrations have been more extensively studied, as discussed above, with the result that the experimental resolution is now $\approx$750 keV (FWHM). The new spectrum is presented below, and in addition, we also show for the first time our $^{7}_{\Lambda}$He results.

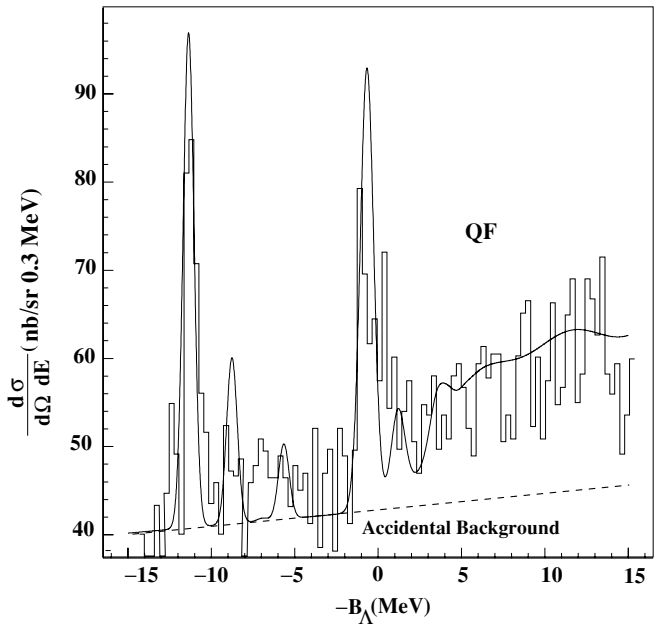

FIG. 7. The binding energy spectrum for $^{12}_{\Lambda}$B electroproduced from a C target. The dashed line is a polynomial fit to the measured accidental background, and the curve is a theoretical calculation, spread as described in the text and overlayed on, not fit to, the data. The bin width was 0.3 MeV.

A. Spectroscopy of $^{12}_{\Lambda}$B hypernuclei

The binding energy spectrum with background of the $^{12}_{\Lambda}$B hypernucleus is shown in Fig. 7. Two prominent structures are obvious in the spectrum, which is similar to that predicted by Motoba *et al*. [23,24] and by Millener [25]. Reference [24] calculates the excitation strengths in DWIA for the photoproduction process of a kaon at an angle of 3° by a 1.3 GeV photon. Our original publication compared the experimental spectrum to a calculation at 0° and a 1.2 GeV photon energy. The curve in Fig. 7 is generated by superimposing Gaussian peaks of the strength and at the energy of each state as obtained from the theoretical prediction. For this superposition, the peak widths are assumed to be 750 keV (FWHM) below and 5 MeV above 15 MeV excitation energy. The background is obtained from a polynomial fit to the averaged accidental background. The positions of the states are taken from Ref. [25], as this latter spectrum was obtained from an effective p shell Λ-nucleus interaction previously matched to (π^+, K^+) data. The reaction strengths [24] for the low-lying states of $^{12}_{\Lambda}$B are shown in Fig. 8. This theoretical curve is directly overlayed on (not fitted to) the data.

Figure 9 shows the number of counts and statistical error in the background subtracted spectrum in order to demonstrate the statistical significance of the data. The major excitations are in good statistical agreement with theory both in position and strength. However, statistics are not sufficient to discuss the core excited state region, lying between the major shell excitations. In comparison to the earlier, published spectrum [14] of this hypernucleus, the resolution and shape of the ground state doublet is improved. The old and new spectra

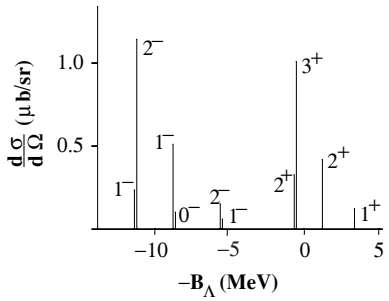

FIG. 8. A schematic representation of the reaction strength for the low lying states of $^{12}_{\Lambda}$B.

are similar with differences that lie within the statistical fluctuations.

The differential cross section can be calculated as if it were photoproduction, by assuming the virtual photons are massless. This averages the elementary (γ,K) reaction at 1500 MeV over the ≈100 MeV spread of virtual gamma energies. The weighted average of the cross section measurements for the ground state doublet at the two incident beam energies is, $140 \pm 17(\text{stat}) \pm 18(\text{sys})$ nb/sr. This value is consistent with the individual values of the separate energy measurements, and also the theoretical photoproduction prediction for this angle and energy [24], 138 nb/sr.

The 2^- component of the ground state doublet is predicted to lie at approximately 150 keV excitation energy, and is expected to be dominant, Fig. 8. The resolution (and statistics) is insufficient to identify this splitting. The 3^+ p-shell state is also predicted to dominate the spectrum in the ≈10 MeV excitation region. While theory indicates the

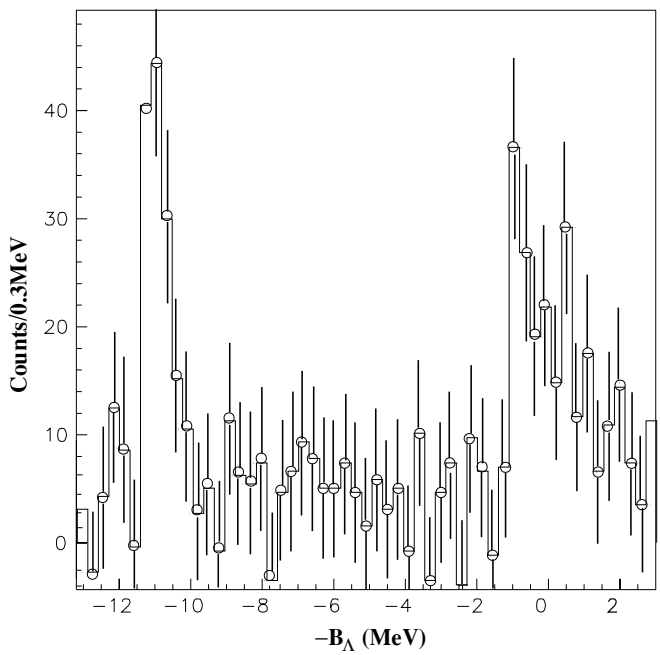

FIG. 9. The spectrum for $^{12}_{\Lambda}$B shown as the number of counts per channel with background subtracted error. This figure should be compared to Fig. 7.

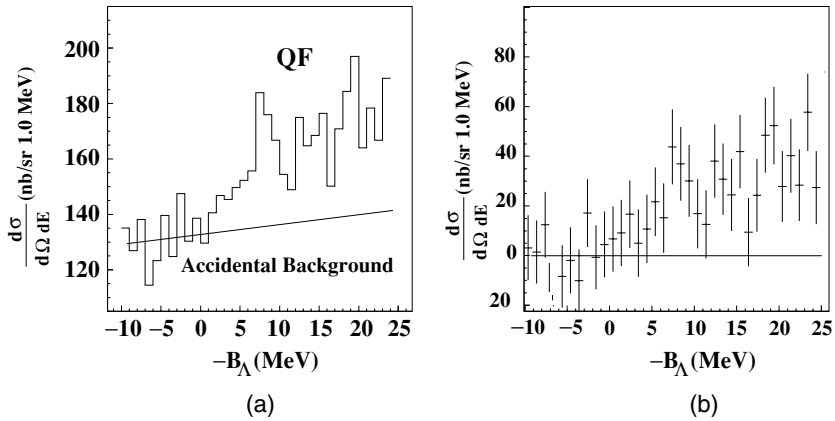

FIG. 10. The binding energy spectrum for ${}^{7}_{\Lambda}$He electroproduced from a ^{7}Li target. The data are binned in 1 MeV intervals. In (a) the zero in the cross section scale is suppressed. (b) shows the background subtracted spectrum with statistical errors.

dominant structure at this excitation energy is actually created by the overlap, Fig. 8, of the 2^+ and 3^+ p-shell states [25]. These two states are not as degenerate in other calculated spectra [24] which use slightly different effective parameters. The newer data suggest that this p-shell peak may be broader than first indicated, but statistics limit the ability to draw specific conclusions. The results do demonstrate sensitivity to the effective interaction and the DWIA transition amplitudes.

The binding energy scale is determined from the position of the Λ and Σ peaks in the calibration spectrum. The ${}^{12}_{\Lambda}$B binding energy is found to be 11.52 ± 0.35 MeV and is in agreement with the accepted value [26] obtained from a measurement using emulsion, 11.37 MeV.

To confirm our cross section normalization, the quasi-free component of the experimental spectrum was extracted, and the yield corrected for acceptance and momentum transfer [27]. We obtained 4.2 interacting protons, in agreement with previous measurements [28,29].

B. Spectroscopy of ${}^{7}_{\Lambda}$He hypernuclei

The measured ${}^{7}_{\Lambda}$He spectrum from the ${}^{7}\mathrm{Li}(e,e'K^+){}^{7}_{\Lambda}\mathrm{He}$ reaction with the accidental background is shown in Fig. 10. Data are binned in 1 MeV intervals to improve statistics, although the experimental resolution is comparable to that obtained in the ${}^{12}_{\Lambda}$B spectrum. The threshold ($B_\Lambda = 0$) is occurs when the the relative velocity between the unbound Λ and the ^{6}He core is zero, i.e., the Λ separation threshold. Negative energies represent bound Λ states, but in this case the ${}^{6}_{\Lambda}\mathrm{He} + n$ and ${}^{5}_{\Lambda}\mathrm{He} + (nn)$ thresholds are some $\approx$2 MeV below the threshold value as defined above. The theoretical prediction [30] of the reaction strengths is shown in Fig. 11. There is little resemblance to the data, although the experimental statistics are poor. For example there is no evidence of any bound state production, although the ground state has a predicted strength of 30 nb/sr. Statistics limit the interpretation of the spectrum as the average statistical error is about 13 nb sr^{-1} MeV^{-1} between -10 and 0 MeV. Using the expected resolution, the total statistical error in the data is approximately 16 nb/sr summed over a 4 σ width about the expected ground state position. As discussed in Refs. [30,31], the cluster structure of the ${}^{7}_{\Lambda}$He hypernuclear system will affect the intrinsic widths of the excited states.

The data may suggest a peak at about 7 MeV above the $\Lambda{}^6$-He threshold, having a statistical uncertainty of about 9% and a width of approximately 3 MeV (FWHM). The background subtracted spectrum with statistical error is shown in Fig. 10. If the enhancement at $\approx$7 MeV in the data corresponds to the superposition of the predicted states near 5 MeV, then the excitation energies are incorrect and the excitation strength is somewhat less than predicted. However the widths of these individual states must be due to their intrinsic values, which are much broader than the experimental resolution. Except for the tail of the quasi-free spectrum, no significant features are observed in the data.

The ${}^{7}_{\Lambda}$He system has two loosely-bound, p-shell neutrons added to a ^{4}He core. The addition of the Λ should significantly perturb the nuclear core, shrinking the nuclear radius. Such a perturbation is observed in the ${}^{7}_{\Lambda}$Li hypernuclear system as a change in the $B(E2)$ gamma transition rate between the $5/2$ and $1/2$ states [9]. Thus one expects to find a ${}^{7}_{\Lambda}$He hypernuclear state [31] bound by about 5 MeV. The ground state masses of the light hypernuclei (s and p shell) are generally determined by the emulsion experiments. In the case of this hypernucleus, the mass distribution from the various emulsion experiments was so broad that a consistent binding energy could not be determined. Isomeric states could explain this broad width [32], as the binding energy was obtained from the energies of the decay products. However

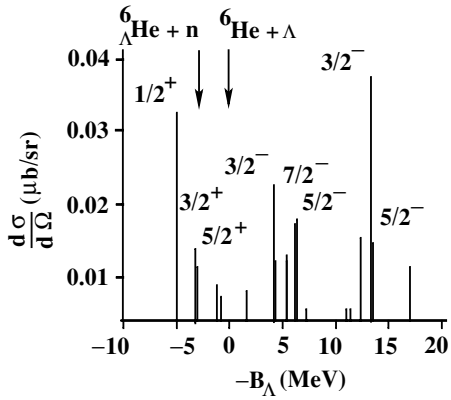

FIG. 11. A schematic representation of the reaction strength for the low lying states of ${}^{7}_{\Lambda}$He.

this would not affect the widths of the reaction peaks in our experiment. Clearly more experimental investigations are needed, as well as better treatments of the structure of ${}^{7}_{\Lambda}$He and the ^{7}Li$(e,e'K^{+})^{7}_{\Lambda}$He reaction mechanism.

IV. CONCLUSION

The first electroproduction experiment using the high quality electron beam at JLab demonstrated sub-MeV energy resolution. For a proof of principle, the experiment used the existing SOS spectrometer in Hall C to measure the reaction kaons even though this spectrometer was not optimized for high resolution. A reanalysis of the previously published data provided a new calibration of the magnetic optics improving the missing mass resolution to a value of 750 keV (FWHM) for the ${}^{12}_{\Lambda}$B spectrum. Variations between the new and the spectrum published earlier lie within the statistical errors. The spectrum is similar to that predicted by theory both in the position and magnitude of the major excitations. However the previously unpublished spectrum of ${}^{7}_{\Lambda}$He is not well reproduced by the existing reaction calculation. The spectra show sensitivity to the effective Λ-nucleus potential parameters.

Since the final state consisted of three recoiling systems, an electron, a kaon, and a missing mass, the resolution in the missing mass depended not only on the the position-to-momentum calibration of the two spectrometers, but on knowledge of the absolute energy and, in principle, the reaction angles. However, because the beam energy and momentum transfer were low and the reaction angles small, contributions from deviations in the angles was small. Thus it was necessary only to calibrate the central momenta and beam energy of the reaction. If larger values of these kinematic parameters had been used, then contributions to the resolution from the error in the knowledge of the reaction angles would have been important. These calibrations were obtained by fitting the position and minimizing the widths of the Λ and Σ peaks produced from the $(e,e'K^{+})$ reaction on protons in a CH_2 target, using the program RAYTRACE to obtain the calibrated magnetic transport elements.

Reaction particle rates in the hadron spectrometer arm (SOS) at the luminosity $4 \times 10^{33}\,\mathrm{cm}^{-2}\,\mathrm{s}^{-1}$ and angle 4° from the C target were 10^5, 1.4×10^3, 140, and $0.4\ \mathrm{s}^{-1}$, for positrons, pions, protons, and kaons, respectively. The positron component was dominated by Dalitz pairs from the target as the SOS spectrometer acceptance included 0°.

High resolution, systematic studies of electroproduced spectra can complement hypernuclear studies by hadronic probes and gamma spectroscopy. The high-quality electron beam at JLab provides new opportunities for future hypernuclear studies with better resolution and much better quality. The present experimental resolution was dominated by the intrinsic resolution of the SOS spectrometer. Improved resolution and count rates are expected in future studies when the SOS is replaced by a dedicated kaon spectrometer having high resolution that is specifically designed for these experiments [33].

ACKNOWLEDGMENTS

Support of the Accelerator and Physics Division staff of the Thomas Jefferson National Accelerator Facility (JLab) is gratefully acknowledged. We wish to thank Dr. D. J. Millener and Dr. T. Motoba for many useful discussions. The Southeastern University Research Association (SURA) operates JLab for the U.S. Department of Energy under Contract No. DE-AC05-84ER40150. This work is also supported in part by research grants from the U.S. Department of Energy and the National Science Foundation, by Monkasho Grant-in-aid for Scientific Research (09304028, 09554007, 12002001), and by the U.S.-Japan collaborative research program under the auspices of the NSF and Japan Society for Promotion of Science.

[1] B. F. Gibson and E. V. Hungerford, III, Phys. Rep. **257**, 349 (1995); A. Gal, Adv. Nucl. Sci. **8**, 1 (1977); B. Povh, Annu. Rev. Nucl. Part. Sci. **28**, 1 (1978).
[2] E. H. Auerbach, A. J. Baltz, C. B. Dover, A. Gal, S. H. Kahana, L. Ludeking, and D. J. Millener, Phys. Rev. Lett. **47**, 1110 (1981).
[3] D. J. Millener, C. B. Dover, and A. Gal, Phys. Rev. C **28**, 2700 (1988); T. Motoba, H. Bando, R. Wunsch, and J. Zofka, *ibid*. **38**, 1322 (1988); D. J. Millener, Nucl. Phys. **A691**, 93c (2001).
[4] M. Prakash *et al*., Phys. Rep. **280**, 1 (1997); De-hua Wen *et al*., Eur. Phys. J. A **21**, 349 (2004); I. Vidañ *et al*., Astron. Astrophys. **399**, 687 (2003).
[5] C. Milner *et al*., Phys. Rev. Lett. **54**, 1237 (1985); P. H. Pile *et al*., *ibid*. **66**, 2585 (1991).
[6] H. Bando, T. Motoba, and Y. Yamamoto, Phys. Rev. C **31**, 265 (1985); T. Motoba, H. Bando, R. Wunsch, and J. Zofka, *ibid*. **38**, 1322 (1988).
[7] T. Hasegawa *et al*., Phys. Rev. Lett. **74**, 224 (1995).
[8] H. Tamura *et al*., Phys. Rev. Lett. **84**, 5963 (2000).
[9] K. Tanida *et al*., Phys. Rev. Lett. **86**, 1982 (2001).
[10] A. S. Rosenthal *et al*., Ann. Phys. (NY) **184**, 33 (1988).
[11] S. R. Cotanch and S. S. Hsiao, Nucl. Phys. **A450**, 419 (1986).
[12] E. V. Hungerford, Prog. Theor. Phys. Supp. **117**, 135 (1994).
[13] T. Motoba, M. Stone, and K. Itonaga, Prog. Theor. Phys. Supp. **117**, 123 (1994); M. Sotona and S. Frullani, Prog. Theor. Phys. Supp. **117**, 151 (1994).
[14] T. Miyoshi *et al*., Phys. Rev. Lett. **90**, 232502 (2003).
[15] T. W. Donnelly and S. R. Cotanch, Proceedings of the 1985 CEBAF Summer Study, 1985; S. S. Hsiao and S. R. Cotanch, Phys. Rev. C **28**, 1668 (1983); S. R. Cotanch and S. S. Hsiao, Nucl. Phys. **A450**, 419 (1986).
[16] G. Xu and E. V. Hungerford, Nucl. Instrum. Methods A **501**, 602 (2003).
[17] C. E. Hyde-Wright, W. Bertozzi, and J. M. Finn, Proceedings of the 1985 CEBAF Summer Workshop, Newport News, VA, 1985.
[18] G. Niculescu *et al*., Phys. Rev. Lett. **81**, 1805 (1998); R. M. Mohring *et al*., Phys. Rev. C **67**, 055205 (2002).
[19] J. E. Spencer and H. A. Enge, Nucl. Instrum. Methods **49**, 181 (1967).

[20] T. Miyoshi *et al*., Nucl. Instrum. Methods A **496**, 362 (2003).
[21] S. Kowalski and H. A. Enge, Nucl. Instrum. Methods A **258**, 407 (1987).
[22] L. Tang, C. Yan, and E. V. Hungerford, Nucl. Instrum. Methods A **366**, 259 (1995).
[23] T. Motoba, M. Sotona, and K. Itonga, Prog. Theor. Phys. Supp. **117**, 123 (1994).
[24] T. Motoba, in *Proceedings of the 8th Conference on Mesons and Light Nuclei*, edited by J. Adams AIP Conf. Proc. No. **603**, 125 (2001); T. Motoba, private communication.
[25] D. J. Millener, in Proceedings of the JLab Workshop on Hypernuclear Physics with Electromagnetic Probes, edited by L. Tang and O. Hashimoto, December 2–4, 1999, Hampton University, Hampton, VA.
[26] M. Jurić, Nucl. Phys. **B52**, 1 (1973).
[27] C. J. Bebek *et al*., Phys. Rev. D **15**, 594 (1977).
[28] W. Hinton, Ph.D. dissertation, Hampton University (1999).
[29] H. Yamazaki *et al*., Phys. Rev. C **52**, R1157 (1995).
[30] O. Richter, M. Sotona, and J. Zofka, Phys. Rev. C **43**, 2753 (1991).
[31] E. Hiyama *et al*., Phys. Rev. C **53**, 2075 (1996)
[32] A. Gal, Adv. Nucl. Phys. **8**, 1 (1975).
[33] JLab proposal E01-011, O. Hashimoto, S. N. Nakamura, L. Tang, and J. Reinhold, spokespersons.